Electron energy loss in ordered arrays of polarizable spheres

Carlos I. Mendoza and Rubén G. Barrera

Instituto de Física, Universidad Nacional Autónoma de Mexico, Apartado Postal 20-364, 01000 Mexico Distrito Federal, Mexico

Ronald Fuchs

Ames Laboratory and Department of Physics and Astronomy, Iowa State University, Ames, Iowa 50011

We develop a theory for the energy loss of swift electrons traveling parallel to an ordered array of polarizable spheres. The energy loss is given in terms of a surface response function which is expressed as a spectral representation. The poles and weights in this representation are determined through the eigenvalues and eigenvectors of an interaction matrix. This matrix takes account of the quasistatic electromagnetic interaction between the polarized spheres to an arbitrary multipolar order. We use our theory to calculate the energy-loss spectra for cubic arrays of aluminum spheres with various numbers of layers and compare the results with those obtained using a dielectric continuum model. [S0163-1829(99)05843-9]

I. INTRODUCTION

Electron-energy-loss spectroscopy (EELS) of inhomogeneous systems has been an active field of research during the last decades. Here, we will be interested in the calculation and analysis of EELS spectra of granular matter. The calculation of the energy loss of swift electrons passing through a system of nanometric inclusions embedded in an otherwise homogeneous matrix was stimulated by the recent experiments of Walsh.[1] The concept of an effective medium for the calculation of the energy-loss function in a granular composite has been very appealing because one might expect that this function could be written in terms of the effective dielectric function associated with the composite. The first attempts along these lines were done by using the effective dielectric functions which had proved to be successful in describing the optical properties of granular composites,[1] like the ones devised, for example, by Maxwell Garnett,[2] Bruggeman,[3] or Landau and Lifshitz.[4] The main problem encountered in using these types of effective dielectric functions was that the peaks in energy loss coming from the excitation of the bulk plasmons of the inclusions did not appear in the calculated spectra. The origin of this problem was the local nature of the effective dielectric response, that is, the effective dielectric response depended only on the frequency of the applied field and had no dependence on its wave vector. This actually means that the response is valid only in the limit as the wave vector tends to zero. Although this limit might be appropriate when the system interacts with light, this is certainly not true when the applied field is the field carried by a moving electron, as in the case of EELS. One would expect that an effective dielectric function that could describe properly the energy-loss process should be nonlocal, that is, should depend on the frequency and the wave vector of the applied field. This approach was taken by Barrera and Fuchs,[5] who find a nonlocal effective dielectric response that could be used to calculate the energy-loss spectra of fast electrons passing through a system of random spherical inclusions contained in a matrix. In their approach, it was assumed that both the spheres and the matrix were

described by local dielectric responses but the interaction among the polarized spheres was taken to all multipolar orders within the mean-field approximation. The calculated spectra using this theory showed well-defined peaks coming from the excitation of the bulk plasmons of the inclusions and the matrix, as well as the ones coming from the excitation of interfacial modes, that is, modes in which the induced charge is located at the interface of the spheres and the matrix. These calculated spectra also agreed with the experimental spectra of Walsh. Further theoretical developments[6] also showed the merits and limitations of an *ad hoc* phenomenological theory[7] devised to explain the experimental results. These developments have also shown the possibility of defining an effective *local* dielectric response that could describe the energy-loss process.

There is also interest in the calculation of energy-loss spectra for an experimental setup in which the electron travels parallel to the surface of the sample. Since there are cases in which it is actually not possible to construct very thin samples, one of the advantages of this experimental setup is that the electron does not have to go through the sample. Nevertheless, there is also the question of how much information about the surface structure will be contained in these energy-loss spectra. Answers to this question have been provided using different approaches. For example, the authors of Ref. 8 have extended to a half space the idea of a nonlocal effective dielectric response discussed above for a system of random spherical inclusions. In order to do this they used a simple model for the structure of the interface together with an *ad hoc* elimination of nonphysical features in the energy-loss spectrum. On the other hand, Pendry and Martín-Moreno[9] (PMM) devised a calculation procedure to obtain the energy-loss spectra of fast electrons traveling parallel to a half space (or a slab) occupied by an *ordered* system of spheres. In this procedure, the fields are decomposed on a transverse basis and the reflection coefficients of the half space are found by a finite-element numerical technique. The energy loss of the electron traveling along a rectilinear classical trajectory above the half space, or a finite slab, is calculated in terms of these reflection coefficients. The cal-

culation includes retardation effects. Although the calculation procedure cannot be readily extended to an infinite system of disordered spheres, the authors argue that their results might also be applied to this case. Nevertheless, the system they actually deal with, that is, a half space of an ordered array of spheres, is interesting in itself. Here, we tackle this problem in the nonretarded limit by finding a spectral representation of the reflection coefficient of longitudinal waves. In terms of this reflection coefficient the energy-loss spectra are readily calculated. Since the interaction among the polarized spheres is kept to all multipolar orders, our calculation can be regarded, in the nonretarded limit, as exact. The most attractive features of our procedure are that: (i) its extension to a disordered system is straightforward and (ii) its numerical solution is extremely simple, as it only requires the calculation of the eigenvalues and eigenvectors of a well-defined interaction matrix. Also, since PMM have not reported results of their numerical calculation for a case in which retardation can be neglected, not only our procedure but also our results are new. In Sec. II we develop the formalism of our theory and derive an explicit expression for the interaction matrix. In Sec. III we present the Maxwell Garnett theory for the case of a finite slab. We apply this theory to specific examples which then serve as a well-defined framework for the analysis of our numerical results. In Sec. IV we present and analyze our numerical results for the case of a single-layer slab. The detailed analysis of this case is then used to construct a clear physical picture of the results presented for a multilayer slab and the half space. Finally, in Sec. V we summarize our results.

II. FORMALISM

We consider a cubic array of identical polarizable spheres of radius a and a local frequency-dependent dielectric function $\epsilon_s(\omega)$ occupying a slab-shaped region of space. The coordinate system is chosen such that the z axis points along the [001] direction of the cubic lattice and the spheres are in the region $z<0$. The xy plane is tangent to the uppermost layer of spheres whose centers lie on the plane $z=-a$. A fast electron is traveling at speed v_I on a rectilinear trajectory above the slab and along the y axis. Its coordinates at time t are given by $(x_0, v_I t, z_0)$, and z_0 is called the impact parameter. The axes of the coordinate system attached to the lattice will be denoted x', y', and z', and they lie along the [100], [010], and [001] crystallographic directions, respectively. The primed and unprimed axes have a common origin and the angle between the x and x' axes will be denoted by ϕ (see Fig. 1). Therefore, the two-dimensional unit cell is a square tilted an angle ϕ from the x axis. In its travel, the electron polarizes the system and the electric field produced by this polarization acts back on the electron. Our objective is the calculation of the power that would be needed by an external force, working against the polarization forces, to keep the electron traveling with a constant speed v_I. Since we are considering very fast electrons, for which the deviation from a rectilinear trajectory is negligible and the change in energy is very small compared with the initial energy, this power can be identified with the power lost by the electron. In our calculation, we will neglect the effects of the magnetic field produced by the moving electron; thus the field pro-
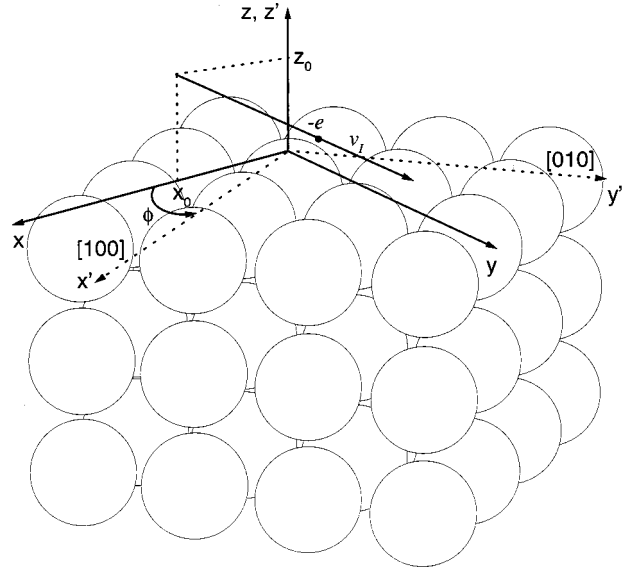

FIG. 1. An electron with charge $-e$ moves with velocity $\mathbf{v}_I = v_I \mathbf{e}_y$ parallel to an ordered array of spheres. The direction [100] of the lattice makes an angle ϕ with respect to the x axis.

duced by the electron will be only its quasistatic longitudinal Coulomb field. This quasistatic approximation will be valid as long as $(v_I/c)^2 \ll 1$, where c is the speed of light.

We now proceed to the calculation of the energy loss. It is convenient to work with Fourier transforms with respect to time and two of the spatial variables. For example, in the region $z<z_0$, the time Fourier transform of the potential produced by external charges located at $z \geq z_0$, which will be called the external potential, satisfies Laplace's equation and can be written as[10]

$$\phi^{ext}(\boldsymbol{\rho},z;\omega) = \int \frac{d^2Q}{(2\pi)^2} \phi^{ext}(\mathbf{Q},\omega) e^{i\mathbf{Q}\cdot\boldsymbol{\rho}+Qz}; \quad z<z_0, \tag{1}$$

where $\boldsymbol{\rho}=(x,y)$, and ω and $\mathbf{Q}=(Q_x,Q_y)$ are the frequency and the two-dimensional wave vector, which are the Fourier variables corresponding to the time and space transforms, respectively. The magnitude of $\mathbf{Q}$ is denoted by $Q\equiv|\mathbf{Q}|$.

Similarly, the induced potential ϕ^{ind} in the region $z>0$ also satisfies Laplace's equation and can be written as

$$\phi^{ind}(\boldsymbol{\rho},z;\omega) = \int \frac{d^2Q}{(2\pi)^2} \phi^{ind}(\mathbf{Q},\omega) e^{i\mathbf{Q}\cdot\boldsymbol{\rho}-Qz}; \quad z>0. \tag{2}$$

Within the spirit of linear response theory we assume a linear relationship between the induced and external potentials, which can be written, in its most general form, as

$$\phi^{ind}(\mathbf{Q},\omega) = -\sum_{\mathbf{Q}'} g(\mathbf{Q},\mathbf{Q}';\omega) \phi^{ext}(\mathbf{Q}',\omega), \tag{3}$$

where the response function $g(\mathbf{Q},\mathbf{Q}';\omega)$ satisfies

$$g(\mathbf{Q},\mathbf{Q}';\omega) = g^*(-\mathbf{Q},-\mathbf{Q}';-\omega), \tag{4}$$

due to the requirement that $\phi^{ind}(\boldsymbol{\rho},z,t)$ should be real if $\phi^{ext}(\boldsymbol{\rho},z,t)$ is real. Here, $*$ denotes complex conjugate and

$g(\mathbf{Q},\mathbf{Q}';\omega)$ plays the role of a (longitudinal) reflection amplitude in analogy to the reflection of transverse waves. In our case, the square-lattice periodicity parallel to the interface allows us to write

$$\phi^{ind}(\mathbf{Q},\omega) = -\sum_{\mathbf{G}} g(\mathbf{Q},\mathbf{Q}+\mathbf{G};\omega)\phi^{ext}(\mathbf{Q}+\mathbf{G},\omega), \quad (5)$$

where $\mathbf{G}$ is a two-dimensional reciprocal lattice vector corresponding to the square lattice.

The energy loss dW of the electron as it moves a distance dy is given by

$$\frac{dW}{dy} = -e \left.\frac{\partial \phi^{ind}(x,y,z,t)}{\partial y}\right|_{x=x_0,y=v_I t,z=z_0}, \quad (6)$$

where $-e$ is the charge of the electron, and $x=x_0$, $y = v_I t$, $z=z_0$ are the equations of its trajectory. For our case where the external charge is a moving electron with charge density $\rho(x,y,z,t) = -e\,\delta(x-x_0)\delta(y-v_I t)\delta(z-z_0)$, the external potential $\phi^{ext}(\mathbf{Q},\omega)$ is given by

$$\phi^{ext}(\mathbf{Q},\omega) = -e(2\pi)^2 \frac{e^{-Qz_0}}{Q} e^{-iQ_x x_0}\delta(\omega-Q_y v_I). \quad (7)$$

Calculating $\phi^{ind}(x,y,z,t)$ using Eqs. (2), (5), and (7), one obtains

$$\frac{dW}{dy} = -i\frac{e^2}{v_I}\int_{-\infty}^{+\infty}\frac{d\omega}{2\pi}\int_{-\infty}^{+\infty} dQ_x \sum_{G_x,G_y} g(\mathbf{Q},\mathbf{Q}+\mathbf{G};\omega)$$
$$\times e^{-Qz_0}\frac{e^{-|\mathbf{Q}+\mathbf{G}|z_0}}{|\mathbf{Q}+\mathbf{G}|}e^{-iG_x x_0}\left(\frac{\omega}{v_I}-G_y\right)e^{-iG_y v_I t}, \quad (8)$$

where

$$\mathbf{Q}=\left(Q_x,\frac{\omega}{v_I}-G_y\right) \quad \text{and} \quad \mathbf{Q}+\mathbf{G}=\left(Q_x+G_x,\frac{\omega}{v_I}\right). \quad (9)$$

One can prove that the above expression for dW/dy is a real quantity by using Eq. (4). One can also see that in this expression there are terms that oscillate in time, which corresponds to a time-dependent energy loss. Since here we are interested only in the time average of the energy loss, this implies that in the sum over G_y only the term with $G_y=0$ will survive. Taking this into account, and transforming the integral over frequency to an integral over positive frequencies in the rhs of Eq. (8) by using the symmetry property (4), one can write

$$\left\langle\frac{dW}{dy}\right\rangle_t = \frac{e^2}{\pi v_I^2}\int_0^{\infty}\omega\,d\omega\sum_{G_x}\int_{-\infty}^{\infty} dQ_x$$
$$\times \text{Im}\left[\frac{g(\mathbf{Q},\mathbf{Q}+\mathbf{G};\omega)}{|\mathbf{Q}+\mathbf{G}|}e^{-iG_x x_0}\right]e^{-Qz_0}e^{-|\mathbf{Q}+\mathbf{G}|z_0}, \quad (10)$$

where $\langle\ldots\rangle_t$ denotes time average, and

$$\mathbf{Q}=\left(Q_x,\frac{\omega}{v_I}\right) \quad \text{and} \quad \mathbf{Q}+\mathbf{G}=\left(Q_x+G_x,\frac{\omega}{v_I}\right). \quad (11)$$

This expression for $\langle dW/dy\rangle_t$ yields the energy loss per unit length for an electron which travels on a rectilinear trajectory along the y axis at a distance z_0 above the interface and at a lateral distance x_0 from the origin. For simplicity, we now suppose that the electron beam, at a given impact parameter z_0, performs a lateral scanning, which corresponds to averaging the electron trajectories over the parameter x_0. This means that in the expression for $\langle dW/dy\rangle_t$ given in Eq. (10), the terms with $G_x\neq 0$ average to zero, leaving only the single term with $G_x=0$. Therefore, we can write

$$\left\langle\frac{dW}{dy}\right\rangle_{t,x_0} = \frac{e^2}{\pi v_I^2}\int_0^{\infty}\omega\,d\omega\int_{-\infty}^{\infty} dQ_x\frac{e^{-2Qz_0}}{Q}\text{Im}\,g(\mathbf{Q};\omega), \quad (12)$$

where $\langle\ldots\rangle_{t,x_0}$ means time and lateral average and

$$g(\mathbf{Q},\omega)\equiv g(\mathbf{Q},\mathbf{Q};\omega). \quad (13)$$

We now write the energy loss $E=\hbar\omega$ and define $d^2P/dldE$, the probability per unit path length, per unit energy, for an electron to be scattered with energy loss E, through

$$\left\langle\frac{dW}{dy}\right\rangle_{t,x_0} = \int_0^{\infty} dE\,E\frac{d^2P}{dldE}. \quad (14)$$

The dimensionless quantity

$$\Xi(E)\equiv\frac{1}{2}m_0 v_I^2 a_0\frac{d^2P}{dldE}, \quad (15)$$

will be referred to as the energy-loss probability function. Here, m_0 is the electron rest mass and a_0 is the Bohr radius. By combining Eqs. (12), (14), and (15) one can finally write

$$\Xi(E)=\frac{1}{2\pi}\int_{-\infty}^{+\infty} dQ_x\frac{e^{-2Qz_0}}{Q}\text{Im}\,g(\mathbf{Q},\omega), \quad (16)$$

where

$$\mathbf{Q}=\left(Q_x,\frac{\omega}{v_I}\right). \quad (17)$$

The next step is the calculation of the response function $g(\mathbf{Q},\omega)$. According to Eq. (3), this implies that we must find the induced potential $\phi^{ind}(\mathbf{Q},\omega)$ with the same $\mathbf{Q}$ as the external potential, that is,

$$\phi^{ind}(\mathbf{Q},\omega) = -g(\mathbf{Q},\omega)\phi^{ext}(\mathbf{Q},\omega). \quad (18)$$

This response function carries information about the interaction among the spheres. Following Ref. 10 the calculation of $g(\mathbf{Q},\omega)$ is performed to all multipolar orders and expressed as a spectral representation in the following form,

$$g(\mathbf{Q},\omega)=-\frac{1}{2}\sum_s\frac{D_s(\mathbf{Q})}{u(\omega)-n_s(\mathbf{Q})}, \quad (19)$$

where

$$u(\omega) = -\frac{1}{\epsilon_s(\omega) - 1} \qquad (20)$$

is the spectral variable, which depends on the dielectric properties of the material. The words *spectral representation* mean that $g(\mathbf{Q},\omega)$ is expressed as a sum of terms with simple poles, where the poles located at $u(\omega_s) = n_s(\mathbf{Q})$ yield the dispersion relations $\omega_s(\mathbf{Q})$ of the polarization modes of the system, and the residues $D_s(\mathbf{Q})$ give the strength of the coupling of these modes with the external potential. Both $n_s(\mathbf{Q})$ and $D_s(\mathbf{Q})$ depend only on the geometry of the system and not on the dielectric properties of the material. The procedure for the calculation of $n_s(\mathbf{Q})$ and $D_s(\mathbf{Q})$ is outlined in Appendix A. It turns out that the $n_s(\mathbf{Q})$ correspond to the

eigenvalues of an interaction matrix

$$H_{lmi}^{l'm'j}(\mathbf{Q}) = \frac{l}{2l+1}\delta_{ll'}\delta_{mm'}\delta_{ij}$$
$$+ \frac{1}{4\pi}\sqrt{ll'}\,a^{l+l'+1}B_{lmi}^{l'm'j}e^{i\mathbf{Q}\cdot(\boldsymbol{\rho}_j - \boldsymbol{\rho}_i)}(1 - \delta_{ij}), \qquad (21)$$

where $B_{lmi}^{l'm'j}$ is a matrix which couples the induced multipolar moment q_{lmi} on sphere i with the induced multipolar moment $q_{l'm'j}$ on sphere j, and it is given by[5,11]

$$B_{lmi}^{l'm'j} = (-1)^{l'+m'}\frac{Y_{l+l',m-m'}^*(\theta_{ij},\varphi_{ij})}{R_{ij}^{l+l'+1}}$$
$$\times \left[\frac{(4\pi)^3(l+l'+m-m')!(l+l'-m+m')!}{(2l+1)(2l'+1)(2l+2l'+1)(l+m)!(l-m)!(l'+m')!(l'-m')!}\right]^{1/2}. \qquad (22)$$

Here, $R_{ij} = |\mathbf{R}_j - \mathbf{R}_i|$ is the distance between sphere j at $\mathbf{R}_j$ and sphere i at $\mathbf{R}_i$, Y_{lm} is the spherical harmonic of order lm, and θ_{ij} and φ_{ij} are the polar and azimuthal angles of the vector $\mathbf{R}_{ij} \equiv \mathbf{R}_j - \mathbf{R}_i$. Notice that the location of the spheres is completely arbitrary in the above expressions, so they can be used for either an ordered or disordered system.

Now, we define the matrix $U_{lmi,s}$ as the matrix that diagonalizes $H_{lmi}^{l'm'j}$, that is,

$$\sum_{lmi,l'm'j} U_{s,lmi}^{-1}H_{lmi}^{l'm'j}U_{l'm'j,s'} = n_s\delta_{ss'}. \qquad (23)$$

Then, one can show (see Appendix A) that the strengths $D_s(\mathbf{Q})$ can be written as

$$D_s(\mathbf{Q}) = \sum_{lmi,l'm'j} A_{Q,lmi}U_{lmi,s}U_{s,l'm'j}^{-1}A_{l'm'j,Q}, \qquad (24)$$

where

$$A_{l'm'j,Q} = \frac{\sqrt{4\pi}}{L}(-i^{m'})e^{-im'\eta}$$
$$\times \sqrt{\frac{l'a^{2l'+1}}{(2l'+1)(l'+m')!(l'-m')!}}Q^{l'-1/2}e^{Qz_j}, \qquad (25)$$

$A_{Q,lmi} = (A_{lmi,Q})^*$, η is the angle of $\mathbf{Q}$ with respect to the x

axis, and L is the size of the system in the x and y directions. These results are exact within the above-mentioned assumptions, and Eqs. (19)–(25) establish a well-defined procedure for the calculation of $g(\mathbf{Q},\omega)$.

Since the size of our system is infinite ($L \to \infty$), the dimension of the interaction matrix would also, strictly speaking, be infinite. Nevertheless, the periodic structure of the system with respect to the x',y' axes allows us to use a small unit cell containing a finite number of spheres and to take account of the rest of the spheres through lattice sums, yielding a modified but finite interaction matrix. For our cubic lattice, the unit cell is a parallelepiped consisting of a pile of n_z cubes, where n_z is equal to the number of layers. In this unit cell, one sphere touches the top side of each cube, and the length L_c of the sides of the cubes is related to the radius a of the spheres by $L_c/a = (4\pi/3f)^{1/3}$, where f is the filling fraction of spheres. It turns out that the contribution of the spheres that are not considered explicitly in the unit cell can be included in the matrix $B_{lmi}^{l'm'j}$ through a lattice sum. This procedure is outlined in Appendix B, and one finds that the interaction matrix $H_{lmi}^{l'm'j}$ can be written as

$$H_{lmi}^{l'm'j}(\mathbf{Q}) = \frac{l}{2l+1}\delta_{ll'}\delta_{mm'}\delta_{ij}$$
$$+ \frac{1}{4\pi}\sqrt{ll'}\,a^{l+l'+1}\widetilde{B}_{lmi}^{l'm'j}e^{i\mathbf{Q}\cdot(\boldsymbol{\rho}_j - \boldsymbol{\rho}_i)}, \qquad (26)$$

where now the indexes i and j denote the location of the spheres *within* the unit cell and

$$\tilde{B}^{l'm'j}_{lmi}=(-1)^{l'+m'}\sum_{\lambda_{x'},\lambda_{y'}}\frac{Y^*_{l+l',m-m'}(\theta_{\mathbf{r}_\lambda+\mathbf{R}_{ij}},\varphi_{\mathbf{r}_\lambda+\mathbf{R}_{ij}})}{|\mathbf{r}_\lambda+\mathbf{R}_{ij}|^{l+l'+1}}e^{i\mathbf{Q}\cdot\mathbf{r}_\lambda}$$

$$\times\left[\frac{(4\pi)^3(l+l'+m-m')!(l+l'-m+m')!}{(2l+1)(2l'+1)(2l+2l'+1)(l+m)!(l-m)!(l'+m')!(l'-m')!}\right]^{1/2}. \tag{27}$$

Here, $\mathbf{r}_\lambda=L_c(\lambda_{x'}\mathbf{e}_{x'}+\lambda_{y'}\mathbf{e}_{y'})$ is a two-dimensional lattice vector of the square lattice, $\lambda_{x'}$ and $\lambda_{y'}$ are integers, and $\mathbf{e}_{x'}$ and $\mathbf{e}_{y'}$ are unit vectors along the x' and y' axes, respectively. The central unit cell (CUC) is located at $(\lambda_{x'}=0,$ $\lambda_{y'}=0)$. The two-dimensonal sums in Eq. (27) were performed using a method described in Ref. 12. The sums are convergent for all values of $\mathbf{Q}$, l, and l'. Similar three-dimensional lattice sums, which depend on a three-dimensional wave vector $\mathbf{k}$, are only conditionally convergent if $l=l'=1$, since the results depend on the direction in which $\mathbf{k}$ approaches zero.

Since we are considering a unit cell with n_z spheres and $-l\leqslant m\leqslant+l$, the order of the interaction matrix is reduced to $N=n_zL_{max}(L_{max}+2)$, where L_{max} is the maximum value of the multipolar moment l included in the calculation. For example, for a slab made of six layers, $(n_z=6)$, and $L_{max}=3$, the order of the interaction matrix is $N=90$.

In the theory we have presented, the array of spherical particles is situated in vacuum. Although we shall show the results of calculations using this geometry, it is unlikely that an EELS experiment could be done with the spheres surrounded by vacuum. Rather, they would be embedded in a matrix with a dielectric function $\epsilon_b(\omega)$. In Appendix C we shall discuss how one can include such a matrix in the theory, and a summary of our result is presented below. We assume that the matrix fills the entire half space $z<0$, and that there is vacuum in the region $z>0$, as before. Of course a physical matrix would not be infinitely thick, but if it is in the form of a layer of material, it should be thick enough $(\gtrsim 50\text{ nm})$ that the effects of its finite thickness are negligible. First, in the calculation of the surface response function using Eqs. (19) and (20), $\epsilon_s(\omega)$ must be replaced by $\epsilon_s(\omega)/\epsilon_b(\omega)$ in Eq. (20), giving a modified surface response function $g_m(\mathbf{Q},\omega)$ in place of $g(\mathbf{Q},\omega)$. Second, if the array of spheres is translated "rigidly" by a distance b in the $-z$ direction, so the centers of the uppermost layer of spheres lie on the plane $z=-(a+b)$, we find $g_b(\mathbf{Q},\omega)=e^{-2Qb}g_m(\mathbf{Q},\omega)$. Finally, in the calculation of $\Xi(E)$ using Eq. (16), the quantity $g(\mathbf{Q},\omega)$ is replaced by

$$g_v(\mathbf{Q},\omega)=\frac{g_b(\mathbf{Q},\omega)[\epsilon_b(\omega)+1]+\epsilon_b(\omega)-1}{g_b(\mathbf{Q},\omega)[\epsilon_b(\omega)-1]+\epsilon_b(\omega)+1}. \tag{28}$$

In Appendix C we also compare our procedure with an alternative method that uses image multipoles.[13,14]

In Sec. IV we will present a numerical solution for $g(\mathbf{Q},\omega)$ for a system of aluminum spheres in vacuum. The dielectric response of aluminum is modeled by a Drude dielectric function

$$\epsilon_s(\omega)=1-\frac{\omega_p^2}{\omega(\omega+i/\tau)}, \tag{29}$$

where ω_p is the plasma frequency and τ the relaxation time. But before looking at the results of our exact theory, it will be illustrative to show the predictions of the Maxwell Garnett effective-medium theory.

III. MAXWELL GARNETT THEORY

In the Maxwell Garnett effective-medium theory our inhomogeneous system is regarded as a homogeneous slab of thickness d with an effective dielectric response $\epsilon_{MG}(\omega)$, given by,[2]

$$\epsilon_{MG}(\omega)=\frac{u(\omega)-(1+2f)/3}{u(\omega)-(1-f)/3}. \tag{30}$$

Here, $u(\omega)$ is the spectral variable defined above [Eq. (20)]. This theory corresponds to a mean-field dipolar approximation, which means that the polarized spheres interact only through their induced average dipole moment.[15]

In the case of aluminum spheres in vacuum, the spectral variable is

$$u(\omega)=\frac{\omega(\omega+i/\tau)}{\omega_p^2}, \tag{31}$$

where we have used the Drude dielectric function given in Eq. (29). On the other hand, the surface response function $g(\mathbf{Q},\omega)$ for a homogeneous slab of thickness d with a local dielectric response $\epsilon(\omega)$ is given by[16]

$$g(Q,\omega)=\frac{[\epsilon^2(\omega)-1](e^{Qd}-e^{-Qd})}{F_-(Q,\omega)F_+(Q,\omega)}, \tag{32}$$

where

$$F_\pm(Q,\omega)=\epsilon(\omega)(e^{Qd/2}\pm e^{-Qd/2})+e^{Qd/2}\mp e^{-Qd/2}. \tag{33}$$

It can be seen that $\text{Im}\,g(Q,\omega)$ has two poles whose frequencies $\omega_\pm(Q)$ are given by

$$\text{Re}\,F_\pm(Q,\omega)=0. \tag{34}$$

These are the dispersion relations of the two normal modes of the electric field within the slab. We now substitute ϵ_{MG} given in Eqs. (30) and (31) into Eq. (32) to get the surface response function $g_{MG}(Q,\omega)$ of our system. In the case $\tau\to\infty$, the dispersion relation $\omega_\pm(Q)$ of the two normal modes can be expressed very simply as
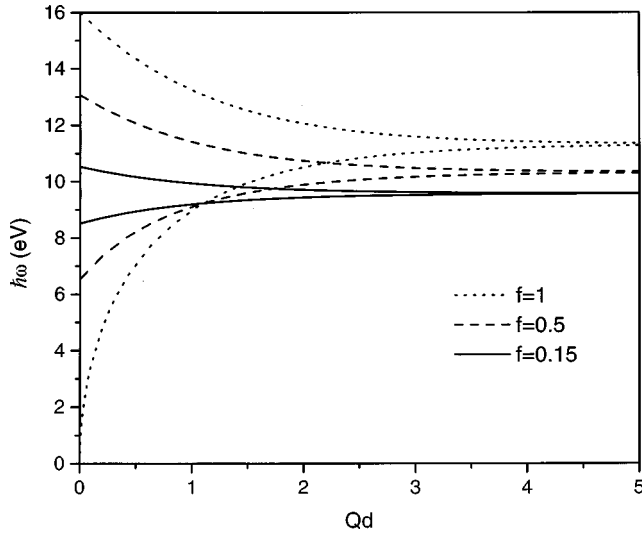
FIG. 2. Dispersion relations, for three different filling fractions, of the two normal modes of the electric field within the slab as given by the Maxwell Garnett theory [Eq. (35)].

$$\omega_\pm^2 = \frac{\omega_p^2}{3}\left[1 + \frac{2 - S_\pm}{1 + S_\pm}f\right], \tag{35}$$

where

$$S_+ = \tanh[Qd/2] \quad \text{and} \quad S_- = \coth[Qd/2]. \tag{36}$$

In the extreme dilute limit ($f\to 0$) one gets $\omega_\pm \to \omega_p/\sqrt{3}$, which corresponds to the dipolar resonance of an isolated metallic sphere. On the contrary, in the limit $f\to 1$ (pure metal), one obtains $\omega_\pm \to \omega_p[1 + S_\pm]^{-1/2}$, which corresponds to the coupled surface-plasmon resonances of the metallic slab. Actually, in a cubic lattice of spheres the limit $f \to 1$ is physically unattainable because for this lattice the maximum possible packing is $f = \pi/6 \approx 0.5236$. Nevertheless, it is interesting that in the Maxwell Garnett theory the $f \to 1$ limit yields the correct results of a pure (local) metal. In the limit $d\to\infty$ (half space) the two modes decouple and one gets $\omega_\pm \to \omega_p/\sqrt{2}$, which is the frequency corresponding to the surface plasmon resonance of the metallic half space.

In Fig. 2 we used Eq. (35) to plot $\omega_\pm$ as a function of Qd for three different filling fractions of aluminum spheres, $f = 0.15$, 0.5, and 1.0, where we have taken $\hbar\omega_p = 16$ eV. The two modes start at frequencies $\omega_+^0 = (\omega_p/\sqrt{3})\sqrt{1 + 2f}$ and $\omega_-^0 = (\omega_p/\sqrt{3})\sqrt{1 - f}$ for $Qd = 0$, approach each other as Qd increases, and join monotonically at $\omega_\infty = (\omega_p/\sqrt{3})\sqrt{1 + f/2}$ for $Qd\to\infty$. For example, for $f = 0.15$, these frequencies are $\hbar\omega_+^0 \approx 10.53$ eV, $\hbar\omega_-^0 \approx 8.52$ eV, and $\hbar\omega_\infty \approx 9.58$ eV, while for $f = 1$, they are $\hbar\omega_+^0 = 16$ eV, $\hbar\omega_-^0 = 0$ eV, and $\hbar\omega_\infty \approx 11.31$ eV. This behavior of the two modes can be understood by noting that as Qd increases, the fields become increasingly concentrated at the surfaces. Therefore, the energy splitting between the modes decreases because there is less interaction between the polarization charges on the two surfaces.

Although the Maxwell Garnett theory (MGT) is based on the dipolar approximation and therefore it should be valid only for small filling fractions, here we present some of its predictions for filling fractions as high as $f = 0.5$. We do this
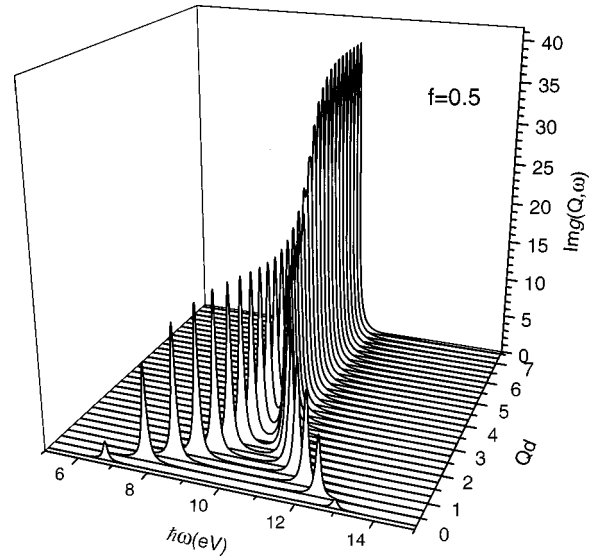

FIG. 3. Surface loss function Im $g(Q,\omega)$, as a function of Qd and $\hbar\omega$, for aluminum spheres in vacuum using the Maxwell Garnett theory and a filling fraction $f = 0.5$.

because the MGT will be taken as a reference for the analysis of our exact results, and in this way it will be illustrative to compare MGT with our results with $L_{\max} = 1$.

In Fig. 3 we show Im g_{MG} as a function of $\hbar\omega$ for $f = 0.5$, and different values of Qd. The Drude parameters used here are $\hbar\omega_p = 16$ eV and $\omega_p\tau = 100$. The curves have a two-peaked structure whose location corresponds to the normal modes frequencies $\omega_\pm$ shown in Fig. 2, and their heights are proportional to the strength of coupling of these normal modes with the external field. There is a very steep growth of both peaks as Qd starts to increase from $Qd = 0$, and the peaks get closer each other as Qd increases further while their height increase more slowly. Finally, for larger values of Qd both peaks merge into one and its height stays almost constant. For smaller values of f, the behavior of Im g_{MG} is similar to the one shown here, although the maximum separation of the peaks at $Qd = 0$ decreases as f decreases, as can be anticipated from Fig. 2.

Now, we use Eq. (16) and Im g_{MG} to calculate the energy-loss probability function $\Xi(E)$. In Fig. 4(a) we show the results of this calculation for $d = 5$ nm, $z_0 = 1$ nm, $f = 0.15$, 0.5, and 1.0, and an electron incident energy $E_I = 100$ keV. One can see that $\Xi(E)$ has a three-peaked structure and how these peaks separate more from each other as f increases. This structure can be easily understood when one realizes that $\Xi(E)$ is obtained by integrating Im $g_{MG}(Q,\omega)$ with respect to $Q_x d$ from $\omega d/v_I$ to ∞, times a decaying weighting function. Thus, the two lateral peaks come from the two peaks in Im g_{MG}, as a function of ω, which are broadened by the shift of these peaks as Qd varies, while the central peak arises from the merging of the two peaks of Im g_{MG} for large values of Qd. For $f = 0.15$, the two lateral peaks get so close to each other that they merge with the central peak, yielding a broad peak with only some reminiscence of its three-peaked structure.

In Fig. 4(b), we show the results for $\Xi(E)$ using the same parameters as before but changing d to $d = 15$ nm. An increase in the thickness d of the slab makes the two lateral
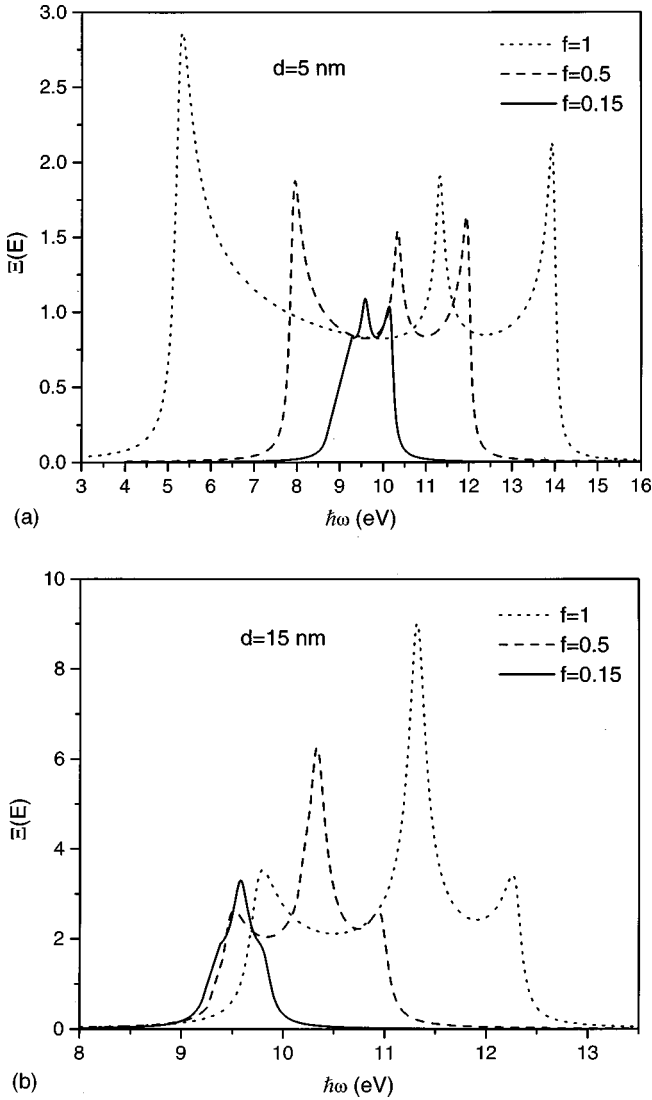
FIG. 4. (a) Energy-loss probability function $\Xi(E)$ as a function of the energy loss $E = \hbar\omega$, for a slab of thickness $d = 5$ nm as obtained using the Maxwell Garnett theory. The solid line corresponds to a filling fraction $f = 0.15$, the dashed line to $f = 0.5$, and the dotted line to $f = 1$. In all the curves an impact parameter $z_0 = 1$ nm was used. (b) The same as in (a) but for $d = 15$ nm.

peaks, in the three-peaked structure of $\Xi(E)$, to get closer to each other, while the height of the middle peak now becomes larger than the height of the lateral ones. The three-peaked structure arises for the same reasons discussed in the previous paragraph, whereas the decrease in splitting between the lateral peaks with increasing thickness d corresponds to the behavior of the two slab modes, as shown in Figs. 2 and 3.

Finally, we note that the peaks in Fig. 4 have been broadened by the finite value of τ. As τ increases the tails at each side of the lateral peaks would tend to disappear, yielding curves with steeper edges and an overall sharper structure. It is important to notice that even in the limit $\tau \rightarrow \infty$ the peaks of $\Xi(E)$ have a broad structure with a finite width. It is only in the limit of the half space ($d \rightarrow \infty$) that the structure of $\Xi(E)$ becomes an isolated delta function at ω_∞ corresponding to the frequency of the surface plasmon of the system.

In the next section, we will see how the results shown here are modified by the exact treatment of the periodic

structure of the lattice. We shall focus our attention on the role played by the two-dimensional periodicity in each layer of spheres.

IV. RESULTS FOR LATTICE OF SPHERES

In this section we present numerical solutions for $\text{Im}\, g(Q, \omega)$ and $\Xi(E)$ based on the procedures given by Eqs. (19)–(27) and Eqs. (15)–(17). In all the results presented below we have chosen a definite set of parameters. For example, the Drude parameters for aluminum have been taken as $\hbar\omega_p = 16$ eV and $\omega_p \tau = 100$. Also, we have fixed $E_I = 100$ keV, which corresponds to the typical incident energies for electrons produced in a scanning transmission electron microscope, and we have chosen $a = 2.5$ nm and $z_0 = 1$ nm. We will show results for systems with different number n_z of layers, and for different values of the following parameters: the filling fraction of the spheres f, the maximum multipolar order L_{max} and the angle ϕ which the electron trajectory makes with the [010] direction of the cubic lattice.

A. Single layer

Here, we present results for a single layer of spheres in a square lattice taking $L_{max} = 1$, which corresponds to the dipolar approximation. In Fig. 5 we plot the dispersion relation $\hbar\omega_s(\mathbf{Q})$ of the three ($s = 1, 2, 3$) normal modes of the electric field in the layer. The angle α gives the direction of $\mathbf{Q}$ with respect to the x' and y' axes through $Q_{x'} = Q \cos\alpha$ and $Q_{y'} = Q \sin\alpha$. We have chosen $f = 0.5$, and two different directions of the vector $\mathbf{Q}$, corresponding to $\alpha = 0°$ and $30°$. The three modes correspond to the eigenvalues of the interaction matrix $H_{1m}^{1m'}$, which is a 3×3 matrix because m (and $m') = -1$, 0, $+1$, and there is one sphere in the two-dimensional unit cell. A comparison of these curves with the ones of Fig. 2, corresponding to $\omega_\pm$ of the MGT, shows that the two-dimensional periodicity in the xy plane introduces a dependence of the dispersion relations $\hbar\omega_s(\mathbf{Q})$ on the direction of $\mathbf{Q}$. For example, when $\alpha = 0°$, $\hbar\omega_s(\mathbf{Q})$ is a periodic function of QL_c with period 2π, while for $\alpha = 30°$ it is not periodic, in agreement with the existence of a square two-dimensional reciprocal lattice. By symmetry, the dispersion relations coincide for $\alpha = 0°$ and $\alpha = 90°$, as well as for $\alpha = 30°$ and $\alpha = 60°$. The physical nature of these modes is determined by the three ($s = 1, 2, 3$) eigenvectors $U_{1m,s}$ of $H_{1m}^{1m'}$. For example, in Fig. 5(a) ($f = 0.5$ and $\alpha = 0°$) the lowest-energy mode, labeled Y, corresponds to a mode polarized along the y' direction, which means that in this mode all the oscillating dipoles point along the y' direction, while the other two modes, labeled X and Z, are polarized along the x' and z directions, respectively. There is no interaction between the different directions of polarization, so the modes preserve their character when they cross. At $QL_c = 0$, the modes with X and Y polarization become degenerate with energy close to 6.53 eV, and the mode with Z polarization has an energy close to 13.06 eV, which correspond to the energies of the two modes in the dispersion relation of the Maxwell Garnett theory at $Qd = 0$, as shown in Fig. 2.

In Fig. 5(b), the parameters are the same as in Fig. 5(a), except that $\alpha = 30°$. An analysis of the eigenvectors $U_{1m,s}$, shows that there is a mode polarized along the z direction,
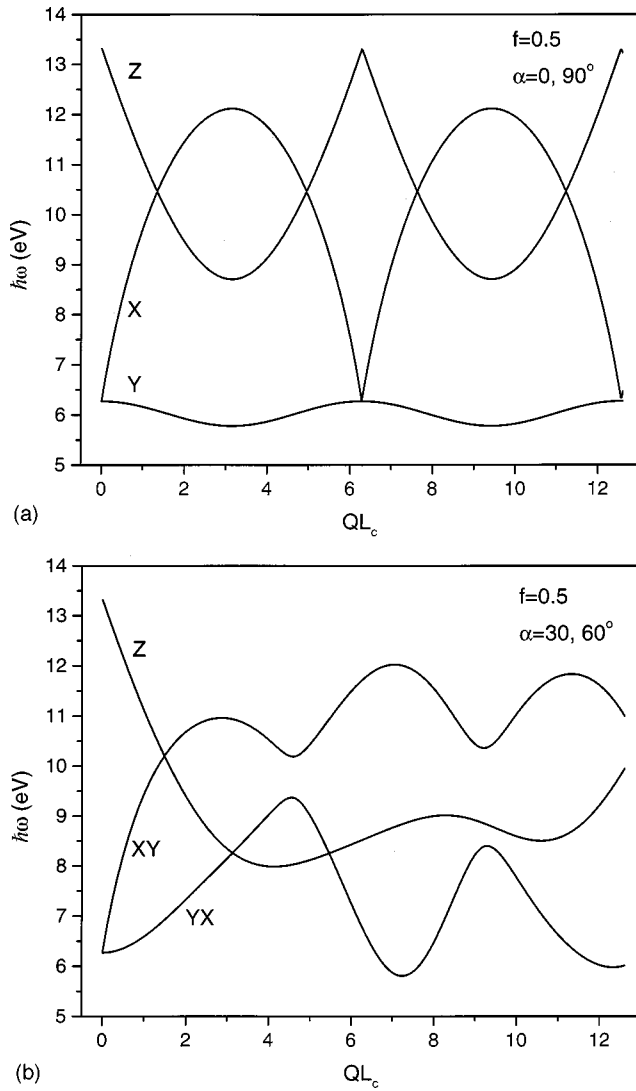
(a)

(b)

FIG. 5. (a) Dispersion relations of the three normal modes of the electric field in a single layer of spheres with $L_{max}=1$. The filling fraction is $f=0.5$ and the vector $\mathbf{Q}$ makes an angle $\alpha=0$ ° (or equivalently $\alpha=90$ °) with respect to the [100] axis of the array of spheres. (b) The same as in (a) but for $\alpha=30$ ° (or equivalently $\alpha=60$ °).

labeled Z, and that this polarization direction is not coupled to that of the other two modes, labeled XY and YX. These two modes are linearly polarized in the xy plane, with polarization directions orthogonal to each other. At $QL_c=0$, the XY and YX modes become degenerate, with an energy equal $\hbar\omega_-^0=6.53$ eV, and the Z mode has an energy equal to $\hbar\omega_+^0=13.06$ eV. Thus, at $QL_c=0$ and at any angle α, both modes have the same energies as the modes at $Qd=0$ in the Maxwell Garnett theory. At $QL_c=0$ the XY mode is polarized along $\mathbf{Q}$, that is, 30 °, and as QL_c increases the angle of polarization decreases, becoming equal to 19 ° at QL_c ≈ 2.0, and -10 ° at $QL_c\approx4.0$.

In Fig. 6 we show $\operatorname{Im} g(Q,\omega)$, for $f=0.5$, as a function of $\hbar\omega$ for different values of QL_c, and $\alpha=0$ and 30 °. In Fig. 6(a), we plot the case $\alpha=0$. There are only two peaks in $\operatorname{Im} g(Q,\omega)$ for each value of QL_c, and the position of these peaks agree with the energies of the corresponding X and Z modes in Fig. 5(a). The heights of the peaks give the strength
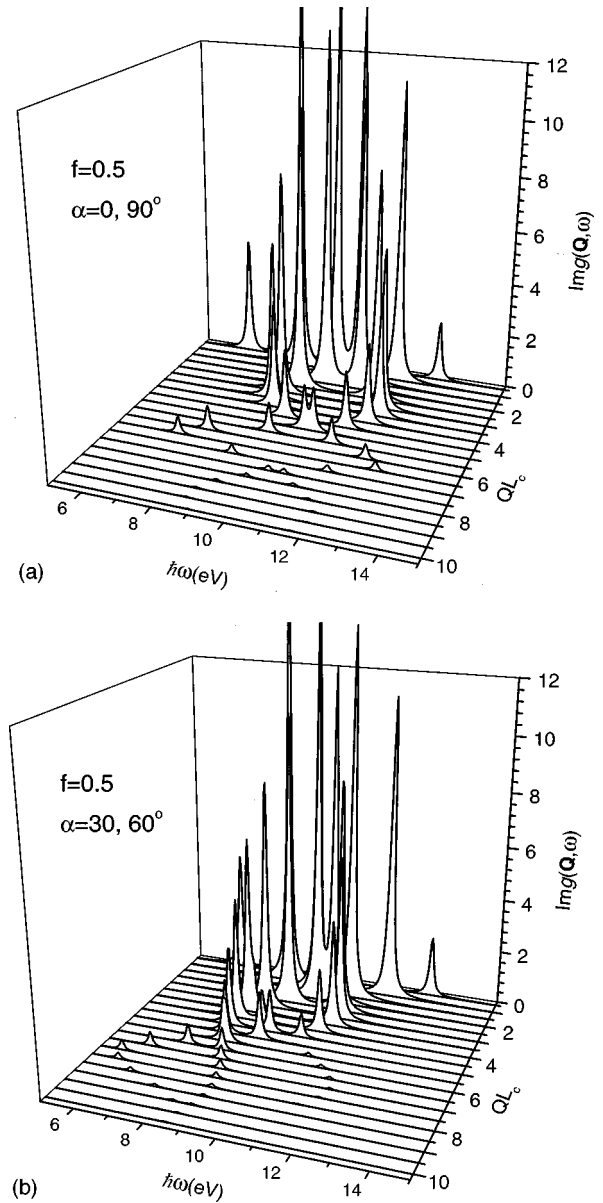

(a)

(b)

FIG. 6. (a) Surface loss function $\operatorname{Im} g(\mathbf{Q},\omega)$, as a function of QL_c and $\hbar\omega$, for a single layer of aluminum spheres in vacuum as given by the numerical calculation with $L_{max}=1$. The filling fraction is $f=0.5$ and the vector $\mathbf{Q}$ makes an angle $\alpha=0$ ° (or equivalently $\alpha=90$ °) with respect to the [100] axis of the array of spheres. (b) The same as in (a) but for $\alpha=30$ ° (or equivalently $\alpha=60$ °).

of the coupling of these modes to the external field. The lowest-energy mode in Fig. 5(a) (labeled Y) does not show up in the plot of $\operatorname{Im} g(Q,\omega)$ because a mode with polarization along the y' direction cannot couple with an external longitudinal field that is confined to the $x'z$ plane. When $\alpha=30$ °, as in Fig. 5(b), two things happen: (i) there are now two modes polarized in the xy plane, as well as a mode polarized in the z direction, and (ii) the external electric field has x', y', and z components. Therefore one expects that three peaks will appear in $\operatorname{Im} g(Q,\omega)$ for all values of QL_c. This is actually what happens, as can be seen in Fig. 6(b), where we plot $\operatorname{Im} g(Q,\omega)$ for $f=0.5$ and $\alpha=30$ °. For both $\alpha=0$ ° and 30 °, the peaks in $\operatorname{Im} g(Q,\omega)$ rise very sharply as QL_c increases at small values of QL_c, then they reach a
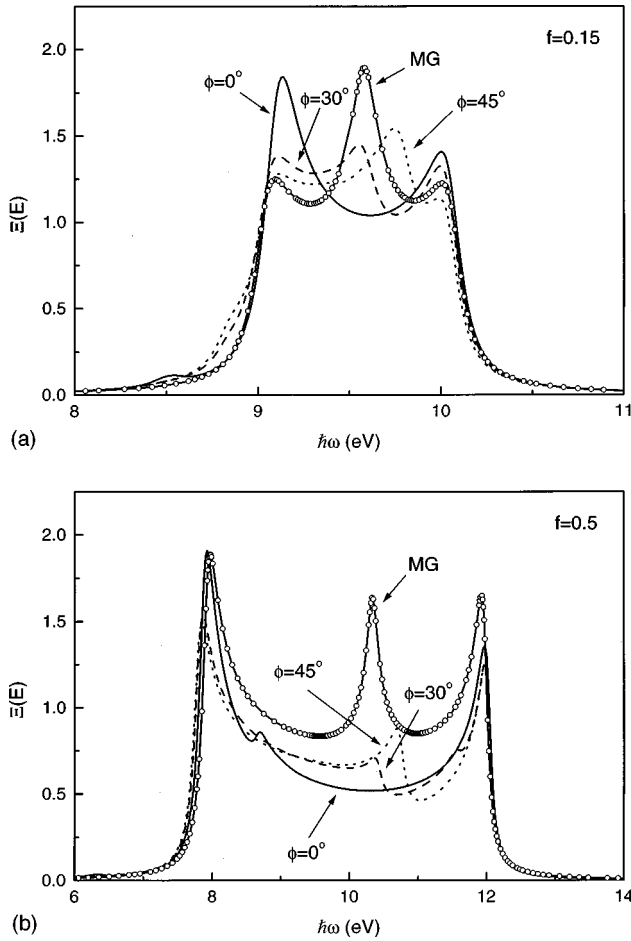
FIG. 7. (a) Energy-loss probability function $\Xi(E)$ as a function of the energy loss $E = \hbar\omega$ for a single layer of spheres with a filling fraction $f = 0.15$ and $L_{max} = 1$. Three different angles of the electron trajectory with respect to the [010] axis of the array of spheres were chosen: $\phi = 0\,^\circ$ (solid line), $30\,^\circ$ (dashed line) and $45\,^\circ$ (dotted line). The open circles represent the corresponding result as given by the Maxwell Garnett theory with $d = 7.58$ nm. (b) The same as in (a) but for $f = 0.5$ and $d = 5.07$ nm.

maximum and decrease as QL_c increases further, becoming almost negligible at $QL_c \approx 10$.

The surface loss function $\mathrm{Im}\, g(Q, \omega)$, whose behavior we have been discussing, can now be used in Eq. (16) to find the energy-loss probability function $\Xi(E)$. In order to carry out the integration over Q_x in Eq. (16) one must define the orientation of the electron trajectory with respect to the lattice. The angle ϕ has been defined as the angle between this trajectory and the [010] direction of the lattice. Recall that the x axis is perpendicular to the electron trajectory, which is in the y direction and x' and y' lie along the [100] and [010] crystallographic directions. Therefore, the integration over Q_x, with a constant value of the component $Q_y = \omega/v_I$, corresponds to a trajectory $Q_{x'} = Q_x \cos\phi - (\omega/v_I)\sin\phi$, $Q_{y'} = (\omega/v_I)\cos\phi + Q_x \sin\phi$ when referred to the x', y' axes. The angle α used in previous sections, defined by $\tan\alpha = Q_{y'}/Q_{x'}$, should not be confused with the trajectory angle ϕ.

In Fig. 7 we have plotted $\Xi(E)$ for $f = 0.15$ and 0.5, $L_{max} = 1$, and three different angles, $\phi = 0\,^\circ$, $30\,^\circ$, and $45\,^\circ$. We also show the corresponding functions $\Xi(E)$ given by

the Maxwell Garnett theory, with $d = L_c$. In the MGT the slab has no structure in the xy plane, so $g_{MG}(\mathbf{Q}, \omega)$ does not depend on the direction of $\mathbf{Q}$ and $\Xi(E)$ is independent of the trajectory angle ϕ.

All the curves for the different values of ϕ, as well as the ones corresponding to the Maxwell Garnett theory, have approximately the same width. This width is determined by the width of the dispersion of the modes as a function of QL_c, and it turns out that the lowest-energy mode and the highest-energy mode correspond, approximately, to the energies of the modes at $Q = 0$. But since these two energies are $\hbar\omega_-^0$ and $\hbar\omega_+^0$, respectively, the width of the spectrum will be the same as the one in the Maxwell Garnett theory for all values of ϕ. One can see also that a change in ϕ modifies the profile a bit, the central maxima and minima change their location, but the size of Ξ remains more or less the same.

In conclusion, we have performed a detailed analysis of the calculation of $\Xi(E)$ for a single ordered layer of spheres in the dipolar approximation and we have shown the differences and similarities of these exact results with the ones obtained in the Maxwell Garnett theory. The inclusion of higher-order multipoles will give rise to a matrix of higher order and, consequently, to a larger number of modes. In this case the analysis of the contribution of all different modes to $\Xi(E)$ will become more complicated and might not further clarify the physics of our problem. Nevertheless, as the number of modes increases the band of energies occupied by the modes also increases. Thus one expects that as the multipolar order is increased the energy band of the modes of the system will become broader until convergence is attained, that is, until the inclusion of additional multipolar orders in the calculation does not change the spectrum of $\Xi(E)$. The multipolar order required to attain convergence is approximately $L_{max} \sim 1 + a/\Delta$, where Δ is the smallest distance between the surfaces of adjacent spheres.[17] This is actually what happens although no figure showing this effect is presented here.

B. Multilayer

Here we consider a system composed of n_z layers of spheres with their centers located, as discussed above, in a cubic lattice. In Figs. 8(a) and 8(b) we show the spectra of $\Xi(E)$ for systems with various values of n_z, f, and L_{max}. We have chosen two filling fractions $f = 0.15$ and $f = 0.30$ and three slabs with number of layers $n_z = 1$, 2, and 6. In all these spectra multipolar convergence has been achieved, and the spectra with the largest number of layers correspond to the semi-infinite half-space limit. For $f = 0.15$, multipolar convergence requires $L_{max} = 3$, while for $f = 0.30$ one has to go up to $L_{max} = 8$.

The energy-loss spectra in Fig. 8 show general features which can be explained easily. For a fixed number of layers n_z, the spectra become broader as f increases. This occurs because the spheres approach each other more closely with increasing f. The most important effect is that the interaction energy between dipoles $\propto 1/r^3$, so the broadening of the spectra due to the dipolar interaction is proportional to f. In addition, as f approaches the close-packed limit, many higher multipoles are involved in the interaction, causing additional broadening of the spectra, as discussed in the previous section.
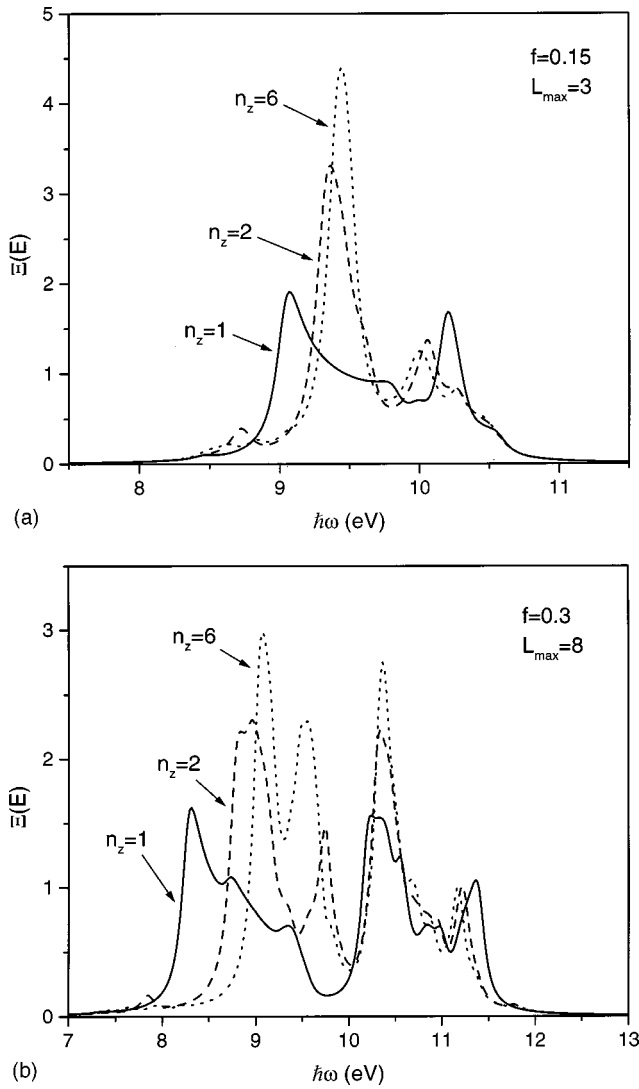
FIG. 8. (a) Energy-loss probability function $\Xi(E)$ as a function of the energy loss $E = \hbar\omega$ for slabs made of n_z layers of spheres and with filling fraction $f = 0.015$. The maximum multipolar order, $L_{max} = 3$, was chosen in order to achieve multipolar convergence. In all curves the angle between the trajectory of the electron and the [010] axis of the array is $\phi = 0°$. The solid line corresponds to $n_z = 1$, the dashed line to $n_z = 2$, and the dotted line to $n_z = 6$. (b) The same as in (a) but with $f = 0.3$ and $L_{max} = 8$.

For a fixed filling fraction f, the spectra become narrower as n_z increases. This occurs because, with an increasing number of layers, the ratio of the number of spheres in the interior of the system to the number in the surface layers increases. A sphere in one of the interior layers is effectively surrounded by a cubic lattice of spheres, and many multipolar interactions between the sphere and its neighbors tend to cancel. This cancellation does not occur for a sphere at or near the surface. In other words, a sphere near the surface interacts more strongly with surrounding spheres through multipoles of all orders, tending to broaden the mode spectrum. Therefore, as the number of layers increases there are fewer spheres at the surface than in the interior, and the spectra become narrower.

It is appropriate to compare our results with those of Pendry and Martín-Moreno (PMM),[9] who also calculated the
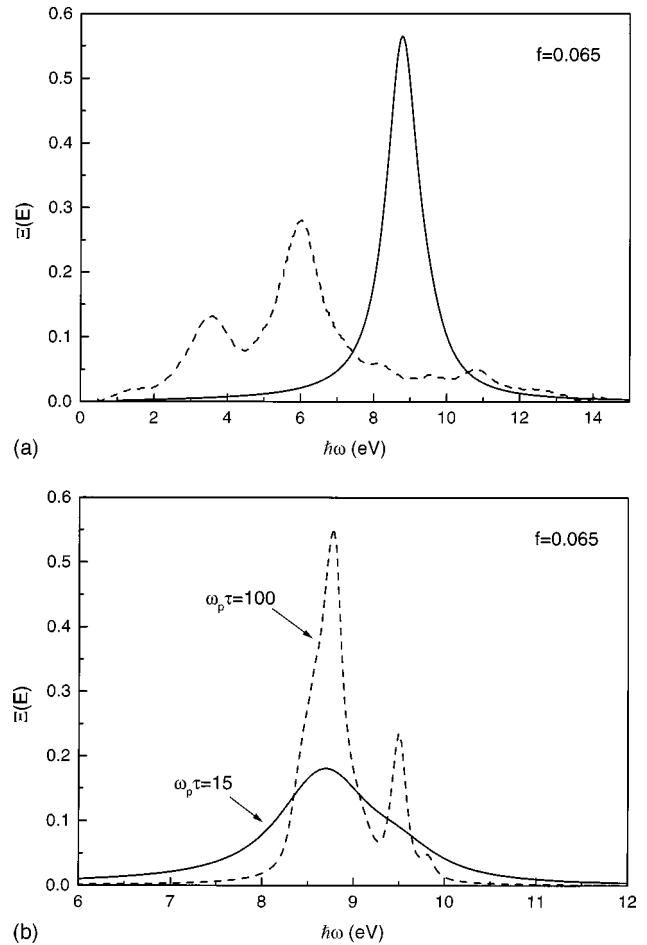
FIG. 9. (a) Energy-loss probability function $\Xi(E)$ as a function of the energy loss $E = \hbar\omega$ for a slab made of $n_z = 6$ layers of spheres and with filling fraction $f = 0.065$. The dashed line corresponds to results of Pendry and Martín-Moreno (PMM) in Ref. 9 and the solid line corresponds to our theory. The angle between the trajectory of the electron and the [010] axis of the array is $\phi = 0°$. The rest of the parameters are the ones reported by PMM in Ref. 9 and quoted in the text. (b) Energy-loss probability function $\Xi(E)$ as a function of the energy loss $E = \hbar\omega$ for a slab made of $n_z = 6$ layers of spheres and with filling fraction $f = 0.065$ according to our theory. The incident energy is $E_I = 3$ keV, the dashed line corresponds to $\omega_p\tau = 100$ and the solid line to $\omega_p\tau = 15$. The rest of the parameters are the ones reported by PMM in Ref. 9 and quoted in the text.

energy-loss spectrum for electrons moving parallel to the surface of a cubic lattice of spheres. They used an impact parameter $z_0 = 1$ nm, aluminum sphere radius $a = 1.25$ nm, filling fraction $f = 0.065$, electron velocity $v_I = 0.4c$, corresponding to $E_I = 46$ keV, a plasma energy 15 eV, and a damping factor $\omega_p\tau = 15$. They did not assume laterally averaged electron trajectories, as we did, but took a definite trajectory along the [100] axis, presumably above a row of spheres. Their calculated energy-loss spectra for six layers is shown in Fig. 9(a). They find a large peak at about 6.0 eV and a smaller peak at 3.7 eV superimposed on a broad background extending from 1 to 13 eV. In Fig. 9(a) we also show the result of our theory, where we have used exactly the same parameters as PMM. Since their results are given in

arbitrary units, we have normalized their curve so the areas under both curves are equal. Their larger peak is at an energy about 2.8 eV lower than our peak at 8.8 eV, and we find no peak that corresponds to their smaller peak.

How can these differences be explained? We do not expect a major difference in the energy-loss spectra for laterally averaged electron trajectories and a single trajectory, since the effective range of interaction between the fast electron and the spheres for an energy-loss $\hbar\omega \lesssim 10$ eV is $v_I/\omega \gtrsim 8$ nm, a distance greater than both the sphere radius and the distance between spheres, $L_c = 5.0$ nm. Moreover, electrons passing directly above a row of spheres will excite sphere modes with higher multipole orders than electrons on laterally averaged trajectories. Since the energy of a mode increases with increasing multipolar order, a single trajectory should give energy loss at a higher energy than laterally averaged trajectories; that is, the difference is in a direction opposite to that observed.

This leaves their inclusion of retardation as a possible explanation for these differences. The numerical calculation of reflection amplitudes from the sphere lattice is an essential step in the theory of PMM, but no details of this calculation are discussed. As we shall explain below, we do not understand how retardation can cause such large downward shifts in peak positions.

A full account of retardation involves additional losses arising from the Cherenkov and Smith-Purcell (SP) radiation from the induced charges, as well as changes in the dispersion relations of surface modes and the coupling to these modes due to the inclusion of the magnetic field. In this discussion, we shall find it useful to represent the array of spheres as a homogeneous half space described by the Maxwell Garnett (MG) effective dielectric response [Eq. (30)]. Since the MG theory neglects any effects of retardation in the response of the individual spheres, such effects will be examined here. When retardation is included, all multipolar surface modes of a sphere become radiative, which causes broadening and shifting to lower energies. These effects are more pronounced for the dipolar mode than for modes of higher multipole orders and become important when the parameter $W = \omega_p a/c \sim 1$.[18] For a sphere radius $a = 1.25$ nm we find $W = 0.09$, a value so small that retardation is unimportant. This is borne out by calculations of the extinction cross section of Al spheres with various radii by Bohren and Huffman.[19] Significant radiative broadening and energy shifts of about 1 eV occur only for much larger sphere radii, $a \sim 20$ nm or $W \sim 1.5$. If $a < 5$ nm these effects are less than 0.1 eV. Therefore, we expect that radiative corrections to the MG theory will be small.

The original explanation of SP radiation involved electrons passing above a metal diffraction grating, the radiation being produced by periodic motion of the induced charges.[20] If one regards the electric field of the moving electron as being described by a set of evanescent waves, the Cherenkov and SP radiation are nothing but the radiation produced by the refraction and diffraction of these waves.[21,22] SP radiation is produced in wavelength ranges $\lambda = L_c(\beta^{-1} \pm 1)/n$ where $n = 1,2, \dots$ and $\beta = v_I/c$. For $\beta = 0.4$, $L_c = 5.0$ nm, and $n = 1$, these wavelengths are 17.5 and 7.5 nm, and the corresponding photon energy range is between 71 and 165 eV. For $n > 1$, photons with even higher energies are pro-

duced. Therefore, the energy-loss spectrum for energies $\lesssim 20$ eV will not be affected by SP radiation.

The energy of Cherenkov radiation can be estimated by using the MG effective dielectric response for the sphere array. The radiation is produced in a frequency window such that $\beta^{-2} < \epsilon_{MG}(\omega) < \infty$. For $\beta = 0.4$ and $f = 0.065$ the corresponding energy window is between 8.2 and 8.4 eV. Since this energy range lies on the low-energy tail of our calculated peak and the ratio of the total radiative energy loss to the longitudinal energy loss is $\sim \beta^2 = 0.16$,[23] we conclude that Cherenkov radiation will not substantially modify our calculated energy-loss spectrum.

If we again approximate the system of spheres by a homogeneous half space described by the MG dielectric function, the inclusion of retardation yields a dispersive surface mode with a frequency ω_s given by $Q^2 c^2/\omega_s^2 = \epsilon_{MG}(\omega_s)/[\epsilon_{MG}(\omega_s) + 1]$. If we set $Q = \omega_s/v_I$, its minimum value, and solve for ω_s, we find an energy 8.76 eV. This energy including retardation is only 0.04 eV lower than the unretarded surface mode energy, 8.80 eV, which is defined by the condition $\epsilon_{MG}(\omega_s) = -1$. PMM give an analytic expression for the energy-loss spectrum of a homogeneous half space including retardation, which yields a peak at a frequency such that $\epsilon(\omega_s) \approx -(1 + \beta^2)$. Taking $\epsilon = \epsilon_{MG}$ we find the energy-loss peak at 8.77 eV, essentially the same result as above.

Other studies of the effects of retardation arrive at similar conclusions.[24] Therefore, the large downward shift of the largest peak by about 2.8 eV for the lattice of spheres is surprising. Also, their smaller peak at 3.7 eV is completely unexplained. We believe that this question could be resolved if PMM were to repeat their calculations for a very low-incident electron energy, e.g., 3 keV, corresponding to $\beta = 0.11$. In this case the effects of retardation are negligible and their resulting spectra could be directly compared with the corresponding ones obtained with our theory. We also suggest that PMM use a larger value of $\omega_p \tau$ in the Drude dielectric response of the Al spheres, say $\omega_p \tau = 100$ or $\hbar \gamma = 0.15$ eV, so that differences in the profiles of the spectra will be more evident. In Fig. 9(b) we show the results of these calculations using our theory for an incident electron energy of 3 keV and $\omega_p \tau = 15$ and 100. These results should be useful for comparison with suggested calculations by PMM.

V. SUMMARY

We have developed a theory for the calculation of the energy-loss probability function of swift electrons traveling parallel to the interface of an ordered array of polarizable spheres. The interaction among the polarized spheres can be calculated to all multipolar orders, and the main assumption of the theory is that the interaction between the electron and the system is only through a longitudinal electric field; that is, retardation effects are neglected.

First, we construct a theory for the response function $g(\mathbf{Q}, \mathbf{Q}'; \omega)$ for spheres at arbitrary positions in a half space, where $\mathbf{Q}$ and $\mathbf{Q}'$ are two-dimensional wave vectors of induced and external potentials, respectively. This response function is expressed as a spectral representation, where the mode positions and strengths are related to the eigenvalues

and eigenvectors of a matrix that describes the interaction between spheres to all multipolar orders. Applying this theory to an ordered array of spheres, the response function assumes the form $g(\mathbf{Q},\mathbf{Q}+\mathbf{G};\omega)$, where $\mathbf{G}$ is a two-dimensional reciprocal lattice vector of the array.

Next, we show how this response function can be used to find the energy-loss probability function for an electron traveling on a definite trajectory outside the array, parallel to its surface, at arbitrary angle with respect to the symmetry directions of the array. Taking an average over lateral positions of the trajectory, we find that only the $\mathbf{G}=\mathbf{0}$ term survives, so the energy loss depends on the distance of the trajectory from the surface and on the trajectory angle, and a simpler response function $g(\mathbf{Q},\boldsymbol{\omega})$ can be used in the energy-loss calculation.

We apply our theory to a sphere array in the form of a slab, where the centers of the spheres are placed on a cubic lattice, and present results for slabs containing 1 to 6 layers of aluminum spheres in vacuum. For a single layer, we show the mode positions in the dipolar approximation for various paths in the $\mathbf{Q}$ plane, and also show graphs of the surface loss function Im $g(\mathbf{Q},\boldsymbol{\omega})$, providing information about both the mode positions and strengths. We present calculations of the energy-loss spectra for various filling fractions of spheres and trajectory angles. We also show that a simplified theory, in which the layer of spheres is replaced by a slab filled with a homogeneous dielectric medium given by the Maxwell Garnett theory, gives energy-loss spectra that agree qualitatively with those found using the exact theory in the dipole approximation.

Our paper ends with calculations of energy-loss spectra for various numbers of sphere layers, with several choices of filling fractions, keeping multipole orders sufficiently high to assure the accuracy of the calculation. We compare our results with those of Pendry and Martín-Moreno, who have done similar calculations for arrays of spheres, but have included retardation; however the differences are so large that we are unable to explain them. We suggest that they repeat their calculation in the unretarded regime in order to compare their results with ours in a region where both theories should be valid.

APPENDIX A: SURFACE RESPONSE FUNCTION

Here we outline the procedure to obtain Eqs. (18)–(25). It is essentially the same procedure as the one described in Ref. 10 but here is extended to the case of anisotropic systems. We first find the response function $g(\mathbf{Q},\mathbf{Q}';\omega)$ defined by Eq. (3) for a system of spheres of radii a_i at arbitrary positions $\mathbf{r}_i$ in the half-space $z<0$.

Let us consider an external potential

$$\phi^{ext}(\mathbf{r},t)=\phi^{ext}(\mathbf{r})e^{-i\omega t}, \tag{A1}$$

oscillating at frequency ω, whose spatial part $\phi^{ext}(\mathbf{r})$ has a single wave-vector component $\mathbf{Q}$ and satisfies Laplace's equation in all regions of space, that is,

$$\phi^{ext}(\mathbf{r})=\phi_0 e^{i\mathbf{Q}\cdot\boldsymbol{\rho}+Qz}. \tag{A2}$$

We now perform a multipole expansion of $\phi^{ext}(\mathbf{r})$ about $\mathbf{r}_i$, the center of the ith sphere,

$$\phi^{ext}(\mathbf{r})=\sum_{lm}\phi^{ext}_{lmi}(r')^l Y_{lm}(\theta',\varphi'), \tag{A3}$$

where $\mathbf{r}'=\mathbf{r}-\mathbf{r}_i$. Here, the coefficient

$$\phi^{ext}_{lmi}=\phi_0\sqrt{4\pi/(2l+1)}\beta_{lm}(-i)^m e^{-im\eta}Q^l e^{i\mathbf{Q}\cdot\boldsymbol{\rho}_i}e^{Qz}, \tag{A4}$$

where $\beta_{lm}=1/\sqrt{(l+m)!(l-m)!}$ and η is the angle which defines the direction of $\mathbf{Q}$: $Q_{x'}=Q\cos\eta$, $Q_{y'}=Q\sin\eta$.

The induced potential acting on sphere i which arises from the multipole moments $q_{l'm'j}$ on all other spheres j can be similarly written in a multipole series

$$\phi^{ind}(\mathbf{r})=\sum_{lm}\phi^1_{lmi}(r')^l Y_{lm}(\theta',\varphi'), \tag{A5}$$

where the coefficients ϕ^1_{lmi} are given by

$$\phi^1_{lmi}=\sum_{l'm'j}B^{l'm'j}_{lmi}q_{l'm'j}. \tag{A6}$$

The multipole moment q_{lmi} is proportional to the lm multipole coefficient of the total potential acting on sphere i, that is,

$$q_{lmi}=-\frac{2l+1}{4\pi}\alpha_{li}(\phi^{ext}_{lmi}+\phi^1_{lmi}), \tag{A7}$$

where α_{li} is the l polarizability of sphere i.[5] We solve Eqs. (A6) and (A7) using the procedure described in Ref. 5. Having solved for the multipole moments on all spheres, we find the induced potential $\phi^{ind}(\mathbf{r})$ and calculate its two-dimensional Fourier transform,

$$\phi^{ind}(\mathbf{Q}',\omega)=\frac{1}{L^2}\int\phi^{ind}(\mathbf{r})e^{Q'z}e^{-i\mathbf{Q}'\cdot\boldsymbol{\rho}}d^2\rho, \tag{A8}$$

where we are assuming a length L of the system in directions parallel to the interface. In carrying out this Fourier transform, we use the identity

$$\int \frac{Y_{lm}(\theta,\varphi)}{r^{l+1}} e^{-i\mathbf{Q}'\cdot\boldsymbol{\rho}} d^2\rho = \sqrt{\frac{2l+1}{4\pi}} \beta_{lm} i^m e^{im\eta'} (Q')^l S,$$

(A9)

where $S=(2\pi/Q')e^{-Q'|z|}$ and the angle η' defines the direction of $\mathbf{Q}'$.

After interchanging $\mathbf{Q}$ and $\mathbf{Q}'$ we find an equation for $\phi^{ind}(\mathbf{Q},\omega)$ in the form of Eq. (3). In this equation the response function $g(\mathbf{Q},\mathbf{Q}';\omega)$ is expressed as a spectral representation

$$g(\mathbf{Q},\mathbf{Q}';\omega) = -\frac{1}{2} \sum_s \frac{D_s(\mathbf{Q},\mathbf{Q}')}{u(\omega)-n_s}.$$

(A10)

The mode positions n_s are eigenvalues of a Hermitian matrix

$$\mathcal{H}_{lmi}^{l'm'j} = \frac{l}{2l+1} \delta_{ll'} \delta_{mm'} \delta_{ij}$$

$$+ \frac{1}{4\pi} \sqrt{ll' a_i^{2l+1} a_j^{2l'+1}} B_{lmi}^{l'm'j}(1-\delta_{ij}),$$

(A11)

and the mode strengths are

$$D_s(\mathbf{Q},\mathbf{Q}') = Q' \sum_{lmi,l'm'j} \mathcal{A}_{\mathbf{Q},lmi} \mathcal{U}_{lmi,s} \mathcal{U}_{s,l'm'j}^{-1} \mathcal{A}_{l'm'j,\mathbf{Q}'}.$$

(A12)

Here,

$$\mathcal{A}_{l'm'j,\mathbf{Q}'} = \sqrt{\frac{4\pi}{L^2}} (-i)^{m'} e^{-im'\eta'}$$

$$\times W_{l'm'}(Q')^{l'-1} a_j^{l'+1/2} e^{i\mathbf{Q}'\cdot\boldsymbol{\rho}_j} e^{Q'z_j},$$

(A13)

with $W_{l'm'} = \sqrt{l'/(2l'+1)(l'+m')!(l'-m')!}$ and $\mathcal{A}_{\mathbf{Q},lmi} = (\mathcal{A}_{lmi,\mathbf{Q}})^*$. The unitary matrix $\mathcal{U}$ diagonalizes $\mathcal{H}$ as in Eq. (23). Finally, Eqs. (18)–(25), which are used to calculate $\langle dW/dy\rangle_{t,x_0}$ for a laterally averaged electron trajectory, are obtained by replacing the sphere radii a_i by a single radius a and setting $\mathbf{Q}'=\mathbf{Q}$.

APPENDIX B: LATTICE SUMS

In this appendix we describe the procedure for deriving Eqs. (26) and (27) from Eqs. (21) and (22). First, we take a finite number of spheres within a central unit cell ($\lambda_{x'}=0$, $\lambda_{y'}=0$), and repeat this cell periodically to generate the infinite system. Then, we split the contribution to the coefficients of the induced potential on sphere i, given by Eq. (A6), into a part coming from the spheres located in the same cell as sphere i (the central unit cell), plus a part coming from the spheres located in the rest of the cells:

$$\phi_{lmi}^1 = \sum_{l'm'j(\neq i)} B_{lmi}^{l'm'j} q_{l'm'j} + \sum_{\lambda \notin CUC} \sum_{l'm'j_\lambda} B_{lmi}^{l'm'j_\lambda} q_{l'm'j_\lambda},$$

(B1)

where the first sum is over spheres $j\neq i$ in the central unit cell (CUC) and the second is a sum over the images j_λ of all spheres in the cell λ. By images we mean the spheres that are generated from a sphere in the CUC by a translation by $\mathbf{r}_\lambda = L_c(\lambda_{x'},\lambda_{y'})$. When considering the images on the λ cells, the interaction of sphere i with its images should be also taken into account. Due to the periodicity in the xy plane the induced multipolar moment on sphere j_λ is related to the induced multipolar moment on sphere j by $q_{lmj_\lambda} = q_{lmj} e^{i\mathbf{Q}\cdot\mathbf{r}_\lambda}$. Then, Eq. (B1) can be written as

$$\phi_{lmi}^1 = \sum_{l'm'j} \left(\sum_\lambda B_{lmi}^{l'm'j_\lambda} e^{i\mathbf{Q}\cdot\mathbf{r}_\lambda} \right) q_{l'm'j}$$

$$= \sum_{l'm'j} \tilde{B}_{lmi}^{l'm'j} q_{l'm'j},$$

(B2)

where we define

$$\tilde{B}_{lmi}^{l'm'j} \equiv \sum_\lambda B_{lmi}^{l'm'j_\lambda} e^{i\mathbf{Q}\cdot\mathbf{r}_\lambda},$$

(B3)

and the sum runs over all the cells except in the case $j=i$, for which the CUC is excluded. Finally, substituting the expression for $B_{lmi}^{l'm'j}$ given in Eq. (22) one gets Eq. (27). Now one follows the procedure described in Appendix A, with $B_{lmi}^{l'm'j}$ replaced by $\tilde{B}_{lmi}^{l'm'j}$, in order to arrive at Eq. (26).

APPENDIX C: SPHERES EMBEDDED IN A DIELECTRIC MATRIX

In this appendix, we discuss the derivation of Eq. (28). The first step is to take the system of spheres located in the half space $z<0$ and replace the vacuum everywhere by the dielectric function of the matrix, $\epsilon_b(\omega)$. Since the surface response function depends on the ratio of the dielectric functions of the two components, the quantity $\epsilon_s(\omega)$ in the spectral variable u defined by Eq. (20) must be replaced by $\epsilon_s(\omega)/\epsilon_b(\omega)$. This changes the surface response function $g(\mathbf{Q},\mathbf{Q}';\omega)$ in Eq. (A10) to a "modified surface response function" $g_m(\mathbf{Q},\mathbf{Q}';\omega)$. In subsequent equations we shall drop the label ω.

Next, if the spheres are moved by a distance b in the $-z$ direction the sphere center positions z_i must be replaced by z_i-b. From Eqs. (A10)–(A13) it can be seen that $g_m(\mathbf{Q},\mathbf{Q}')$ is changed to $g_b(\mathbf{Q},\mathbf{Q}') \equiv e^{-(Q+Q')b} g_m(\mathbf{Q},\mathbf{Q}')$.

Finally, we must replace the dielectric matrix in the $z>0$ half space by vacuum, and find the surface response function $g_v(\mathbf{Q})$ of the system as seen from the vacuum. If we take a single Fourier component $\mathbf{Q}$ for the external potential in the vacuum and assume that the system is periodic, so the wave vectors $\mathbf{Q}$ and $\mathbf{Q}'$ differ by a reciprocal lattice vector $\mathbf{G}$, expressions for the potential in the vacuum and just inside the matrix are, respectively,

$$V^{(1)} = e^{i\mathbf{Q}\cdot\boldsymbol{\rho}} e^{Qz} - \sum_{\mathbf{G}} g_v(\mathbf{Q}+\mathbf{G},\mathbf{Q}) e^{i(\mathbf{Q}+\mathbf{G})\cdot\boldsymbol{\rho}} e^{-|\mathbf{Q}+\mathbf{G}|z};$$

$$z>0, \quad \text{(C1)}$$

$$V^{(2)} = \sum_{\mathbf{G}} [a_{\mathbf{Q}+\mathbf{G}} e^{|\mathbf{Q}+\mathbf{G}|z} + b_{\mathbf{Q}+\mathbf{G}} e^{-|\mathbf{Q}+\mathbf{G}|z}] e^{i(\mathbf{Q}+\mathbf{G})\cdot\boldsymbol{\rho}};$$

$$0 > z > -b. \quad (\text{C2})$$

The unknown coefficients $b_{\mathbf{Q}+\mathbf{G}}$, which are Fourier components of the induced potential in the region between the vacuum-matrix interface and the spheres, can be expressed in terms of $a_{\mathbf{Q}+\mathbf{G}}$, the unknown external potential coefficients in the same region:[25]

$$b_{\mathbf{Q}+\mathbf{G}} = -\sum_{\mathbf{G}'} g_b(\mathbf{Q}+\mathbf{G}, \mathbf{Q}+\mathbf{G}') a_{\mathbf{Q}+\mathbf{G}'}. \quad (\text{C3})$$

From the continuity of the potential and the normal component of the displacement at the interface $z=0$, we find two sets of equations,

$$\delta_{\mathbf{G},0} - g_v(\mathbf{Q}+\mathbf{G}, \mathbf{Q}) = a_{\mathbf{Q}+\mathbf{G}} - \sum_{\mathbf{G}'} g_b(\mathbf{Q}+\mathbf{G}, \mathbf{Q}+\mathbf{G}') a_{\mathbf{Q}+\mathbf{G}'}, \quad (\text{C4})$$

$$\delta_{\mathbf{G},0} + g_v(\mathbf{Q}+\mathbf{G}, \mathbf{Q})$$
$$= \epsilon_b \left[a_{\mathbf{Q}+\mathbf{G}} + \sum_{\mathbf{G}'} g_b(\mathbf{Q}+\mathbf{G}, \mathbf{Q}+\mathbf{G}') a_{\mathbf{Q}+\mathbf{G}'} \right]. \quad (\text{C5})$$

For $\mathbf{G} \neq 0$, the sum of Eqs. (C4) and (C5) gives

$$\frac{\epsilon_b+1}{\epsilon_b-1} a_{\mathbf{Q}+\mathbf{G}} + \sum_{\mathbf{G}'} g_b(\mathbf{Q}+\mathbf{G}, \mathbf{Q}+\mathbf{G}') a_{\mathbf{Q}+\mathbf{G}'} = 0; \quad \mathbf{G} \neq 0. \quad (\text{C6})$$

If the $\mathbf{G}'=0$ term is taken out of the sum in Eq. (C6) and moved to the right-hand side, the coefficents $a_{\mathbf{Q}+\mathbf{G}}$ can be solved in terms of $a_{\mathbf{Q}}$. Defining the matrix

$$T_{\mathbf{GG}'} = \frac{\epsilon_b+1}{\epsilon_b-1} \delta_{\mathbf{GG}'} + g_b(\mathbf{Q}+\mathbf{G}, \mathbf{Q}+\mathbf{G}'); \quad \mathbf{G}, \mathbf{G}' \neq 0, \quad (\text{C7})$$

the solution can be written using the inverse of T:

$$a_{\mathbf{Q}+\mathbf{G}'} = -\sum_{\mathbf{G}\neq 0} [T^{-1}]_{\mathbf{G}'\mathbf{G}} g_b(\mathbf{Q}+\mathbf{G}, \mathbf{Q}) a_{\mathbf{Q}}; \quad \mathbf{G}' \neq 0. \quad (\text{C8})$$

If we use Eq. (C8) for the coefficients $a_{\mathbf{Q}+\mathbf{G}'}$ in Eqs. (C4) and (C5) with $\mathbf{G}=0$ the result is

$$1 - g_v(\mathbf{Q}) = a_{\mathbf{Q}}[1 - g_b(\mathbf{Q}) + W(\mathbf{Q})], \quad (\text{C9})$$

$$1 + g_v(\mathbf{Q}) = \epsilon_b a_{\mathbf{Q}}[1 + g_b(\mathbf{Q}) - W(\mathbf{Q})], \quad (\text{C10})$$

where $g_v(\mathbf{Q}) \equiv g_v(\mathbf{Q},\mathbf{Q})$, $g_b(\mathbf{Q}) \equiv g_b(\mathbf{Q},\mathbf{Q})$, and

$$W(\mathbf{Q}) = \sum_{\mathbf{G},\mathbf{G}'\neq 0} g_b(\mathbf{Q}, \mathbf{Q}+\mathbf{G}') [T^{-1}]_{\mathbf{G}'\mathbf{G}} g_b(\mathbf{Q}+\mathbf{G}, \mathbf{Q}). \quad (\text{C11})$$

Finally, solving Eqs. (C9) and (C10) for $g_v(\mathbf{Q})$, and neglecting $W(\mathbf{Q})$, we get Eq. (28).

We can show that $W(\mathbf{Q})$ can be neglected under the following conditions: (a) $v_I/\omega \gtrsim 2L_c$; (b) $z_0 \gtrsim L_c/5$; (c) $b \gtrsim L_c/4$. Condition (a) states that the effective interaction

range of the incident electron must be appreciably larger than the distance between spheres; conditions (b) and (c) state that neither the electron trajectory nor the spheres should be too close to the vacuum-matrix interface. Conditions (a) and (b) imply that in Eq. (12) the integration trajectory lies close to origin $\mathbf{Q}=0$ and that the factor $Q^{-1}\exp(-2Qz_0)$ in the integrand falls off rapidly as $|Q_x|$ increases, so that less than $1/20$ of the contribution to the integral occurs for $Q > G_0/2$, where $G_0 \equiv 2\pi/L_c$ is the reciprocal lattice unit vector. Therefore, for the small values of Q which contribute significantly to the integral in Eq. (12), we have $|\mathbf{Q}+\mathbf{G}| \sim G$ and $|\mathbf{Q}+\mathbf{G}'| \sim G'$, so from Eqs. (A10)–(A13) it follows that $|g_b(\mathbf{Q},\mathbf{Q}+\mathbf{G}')g_b(\mathbf{Q}+\mathbf{G},\mathbf{Q})| \lesssim \exp(-2bG_0)g_b(\mathbf{Q})$, and from Eq. (C11) we get $|W(Q)| \lesssim \exp(-2bG_0)|g_b(\mathbf{Q})|$. We have assumed that $|g_b(\mathbf{Q})| \sim 1$ and that the terms in Eq. (C11) have many different phases in the complex plane. Condition (c) implies that $|W(Q)| \lesssim 0.04|g_b(\mathbf{Q})|$. It can also be shown that if $\epsilon_b \sim -1$, so the terms $[(\epsilon_b+1)/(\epsilon_b-1)]\delta_{\mathbf{GG}'}$ in $T_{\mathbf{GG}'}$ are small, then condition (c) must be replaced by $b \gtrsim L_c/2$. Also, the assumption $|g_b(\mathbf{Q})| \sim 1$ will not be valid near resonances of $g_b(\mathbf{Q})$, so Eq. (28) cannot be expected to reproduce correctly all fine details of energy-loss peaks which might appear when the damping factor is small.

The evaluation of $W(\mathbf{Q})$ is difficult; therefore, if the conditions for neglecting $W(\mathbf{Q})$ are not satisfied, an alternative method for taking account of the dielectric matrix, that of image multipoles, may be useful.[13,14] Here, each sphere has an image formed by the vacuum-matrix interface. The interaction between the spheres and their images is taken into account from the beginning, and appears in the multipolar interaction, Eq. (A6). The coeffients $B_{lmi}^{l'm'j}$ will include the potential produced by the image multipoles, so these coefficients, as well as $\mathcal{H}_{lmi}^{l'm'j}$ [Eq. (A11)] now depend on $\epsilon_b(\omega)$. If $\epsilon_b(\omega)$ is dissipative, the eigenvalues n_s of $\mathcal{H}_{lmi}^{l'm'j}$ will be complex, and will depend on ω. The spectral representation method loses much of its attractiveness, and it may be preferable to solve Eqs. (A6) and (A7) for the unknown q_{lmi} directly by matrix inversion.[13] If the spheres are very close to the interface, both methods will have difficulties: in our method, many $\mathbf{G}, \mathbf{G}'$ terms will contribute to $W(\mathbf{Q})$, and in the image multipole method, many high-order multipoles must be kept.

If the spheres are embedded in a dielectric slab, our method must be extended to include transmission response functions, whereas the image multipole method will involve an infinite series of images.[14]

Since no experiments have been done with ordered spheres in a matrix, we have not presented calculations using Eq. (28) with particular matrix dielectric functions. Nevertheless, it is instructive to consider a simple example: a semi-infinite system of small Al spheres, described by the Maxwell Garnett effective dielectric function, with a nondispersive dielectric function $\epsilon_b = 2$ for the matrix. If the spheres are in vacuum, there is a single energy-loss peak at 10.7 eV for $f=0.4$ and at 9.2 eV for $f \sim 0$. When the dielectric matrix is included, the energy-loss peak shifts to 8.2 eV for $f=0.4$ and to 7.2 eV for $f \sim 0$. If dielectric function of the matrix is dispersive, its effects can be much more complicated; in particular, there can be additional energy-loss peaks associated with dielectric-vacuum interfacial surface modes.

[1] C. A. Walsh, Philos. Mag. A **59**, 227 (1989).

[2] J. C. Maxwell Garnett, Philos. Trans. R. Soc. London **203**, 385 (1904).

[3] D. A. G. Bruggeman, Ann. Phys. (Leipzig) **24**, 636 (1935).

[4] L. D. Landau and E. M. Lifshitz, *Electrodynamics of Continuous Media* (Pergamon, New York, 1960).

[5] R. G. Barrera and R. Fuchs, Phys. Rev. B **52**, 3256 (1995).

[6] R. Fuchs, R. G. Barrera, and J. L. Carrillo, Phys. Rev. B **54**, 12 824 (1996).

[7] A. Howie and C. Walsh, Microsc. Microanal. **2**, 171 (1991).

[8] C. I. Mendoza, R. G. Barrera, and R. Fuchs, Phys. Rev. B **57**, 11 193 (1998).

[9] J. B. Pendry and L. Martín-Moreno, Phys. Rev. B **50**, 5062 (1994).

[10] R. Fuchs, C. I. Mendoza, R. G. Barrera, and J. L. Carrillo, Physica A **241**, 29 (1997).

[11] R. Fuchs and F. Claro, Phys. Rev. B **39**, 3875 (1989).

[12] B. R. A. Nijboer and F. W. De Wette, Physica (Amsterdam) **23**, 309 (1957).

[13] L. Fu, P. B. Macedo, and L. Resca, Phys. Rev. B **47**, 13 818 (1993).

[14] L. Fu and L. Resca, Physica A **241**, 17 (1997). This paper has a typographical error in Eqs. (1c): the factor 2 in the denominators of both equations should be deleted.

[15] R. G. Barrera, G. Monsivais, and W. L. Mochán, Phys. Rev. B **38**, 5371 (1988).

[16] P. M. Echenique and J. B. Pendry, J. Phys. C **8**, 2936 (1975).

[17] F. Claro, Solid State Commun. **49**, 229 (1984).

[18] R. Fuchs and K. L. Kliewer, J. Opt. Soc. Am. **58**, 319 (1968).

[19] C. F. Bohren and D. R. Huffman, *Absorption and Scattering of Light by Small Particles* (Wiley, New York, 1983), p. 338.

[20] S. J. Smith and E. M. Purcell, Phys. Rev. **92**, 1069 (1953).

[21] G. Toraldo di Francia, Nuovo Cimento **16**, 61 (1960).

[22] V. P. Shestopalov, *The Smith-Purcell Effect* (Nova Science Publishers, New York, 1998).

[23] J. D. Jackson, *Classical Electrodynamics* (Wiley, New York, 1975), Eqs. (13.36) and (13.79).

[24] A. Otto, Phys. Status Solidi **22**, 401 (1967); R. H. Milne, and P. M. Echenique, Solid State Commun. **55**, 909 (1985); R. García-Molina, A. Gras-Marti, A. Howie, and R. H. Ritchie, J. Phys. C **18**, 5335 (1985).

[25] The external potential in this region includes both the ''true'' external potential $e^{i\mathbf{Q}\cdot\boldsymbol{\rho}}e^{Qz}$ and the potential whose source is the polarization charge on the vacuum-matrix interface; this is the physical explanation of the occurrence of coefficients $a_{\mathbf{Q}+\mathbf{G}}$ with $\mathbf{G}\neq 0$.